

Depth-Weighted Detection of Behaviours of Risk in People with Dementia using Cameras

Pratik K. Mishra, Irene Ballester, Andrea Iaboni, Bing Ye, Kristine Newman, Alex Mihailidis, and Shehroz S. Khan

Abstract—The behavioural and psychological symptoms of dementia, such as agitation and aggression, present a significant health and safety risk in residential care settings. Many care facilities have video cameras in place for digital monitoring of public spaces, which can be leveraged to develop an automated behaviours of risk detection system that can alert the staff to enable timely intervention and prevent the situation from escalating. However, one of the challenges in our previous study was the presence of false alarms due to disparate importance of events based on distance. To address this issue, we proposed a novel depth-weighted loss to enforce equivalent importance to the events happening both near and far from the cameras; thus, helping to reduce false alarms. We further propose to utilize the training outliers to determine the anomaly threshold. The data from nine dementia participants across three cameras in a specialized dementia unit were used for training. The proposed approach obtained the best area under receiver operating characteristic curve performance of 0.852, 0.81 and 0.768, respectively, for the three cameras. Ablation analysis was conducted for the individual components of the proposed approach and effect of frame size and frame rate. The performance of the proposed approach was investigated for cross-camera, participant-specific and sex-specific behaviours of risk detection. The proposed approach performed reasonably well in reducing false alarms. This motivates further research to make the system more suitable for deployment in care facilities.

Index Terms—Dementia, Behaviours of risk, Agitation, Video, Autoencoder, Anomaly Detection, Deep Learning.

This paragraph of the first footnote will contain the date on which you submitted your paper for review. This work was supported by AGE-WELL NCE Inc, Alzheimer's Association, Natural Sciences and Engineering Research Council, UAE Strategic Research Grant, Walter and Maria Schroeder Institute for Brain Innovation and Recovery and the European Union's Horizon 2020 research and innovation programme under MSCA grant agreement number 861091 for the visuAAL project.

Pratik K. Mishra, Alex Mihailidis and Shehroz S. Khan are with KITE, Toronto Rehabilitation Institute, Toronto, ON, Canada, and Institute of Biomedical Engineering, University of Toronto, Toronto, ON, Canada (e-mail: pratik.mishra@mail.utoronto.ca; alex.mihailidis@utoronto.ca; shehroz.khan@uhn.ca).

Irene Ballester is with Computer Vision Lab, TU Wien, 1040 Vienna, Austria (e-mail: irene.ballester@tuwien.ac.at)

Andrea Iaboni is with KITE, Toronto Rehabilitation Institute, Toronto, ON, Canada, and Department of Psychiatry, Temerty Faculty of Medicine, University of Toronto, Toronto, ON, Canada. (e-mail: andrea.iaboni@uhn.ca)

Bing Ye is with KITE, Toronto Rehabilitation Institute, Toronto, ON, Canada. (e-mail: bing.ye@utoronto.ca)

Kristine Newman is with Daphne Cockwell School of Nursing, Toronto Metropolitan University, Toronto, ON, Canada. (e-mail: kristine.newman@torontomu.ca)

I. INTRODUCTION

People living with dementia (PwD) can develop behavioural and psychological symptoms putting themselves and the people around them at risk. These behaviours of risk include pacing, pushing, hitting, kicking, intentional falling, and other behaviours that are self-harming, or harmful to others [1]. Long term care (LTC) homes often suffer from understaffing [2] making it challenging for the staff to continuously oversee the safety of the residents. Video cameras are an unobtrusive and inexpensive alternative for monitoring behaviour as they are already used by many LTC homes for security purposes, saving the time and expense of additional infrastructure installation. Video cameras are rich in vital spatio-temporal information, which can be leveraged using deep learning approaches to design automated behaviours of risk detection systems that can be used to alert the staff in real-time and enable timely and appropriate interventions. This has important implications for safety and for helping to better understand the nature and triggers of the behaviours.

Behaviours of risk detection is a challenging problem due to their diversity and rare occurrence, making supervised classification approaches inappropriate. An anomaly detection approach is more plausible, where a method can be trained to learn the normal behaviour characteristics and identify high variation cases as anomalies during testing [3]. In our previous work [4], a spatio-temporal autoencoder was used to detect behaviours of risk as anomalies. However, there were significant issues with false positives (or false alarms), that could cause usability issues. In general, video anomaly detection (VAD) autoencoder approaches can become sensitive to the background, leading to high reconstruction errors when a major part of the background is blocked [5]. The objects or people closer to the camera cover a larger portion of the background than those further away, leading to significantly higher reconstruction errors and causing increased false positives. To tackle this problem, we propose a novel loss where the depth of the pixels is used as weight to diminish the overshadowing effect caused by the larger area of the people/objects close to camera. The aim is to reduce false positives by enforcing equivalent importance in analyzing the events happening in the unit irrespective of the distance to camera. In the absence of anomalies in the training set, we propose to utilize unusual activities that are not behaviours of risk, such as large objects or crowded scenes as proxy outliers to determine a threshold for

detecting behaviours of risk. Expanding on our previous work [4] that analyzed behaviours of risk in one dementia participant using a single camera, here we extend the analysis to nine participants and three cameras. The performance for detecting behaviours of risk can vary across individuals depending upon the type of behaviours of risk, number of episodes recorded and demographic variables such as sex. To address this variability, we also conduct participant-specific and sex-specific analyses of the effectiveness of detecting behaviours of risk by the proposed approach. The main contributions of this work are:

- 1) We propose an approach using a novel depth-weighted loss to enforce equivalent importance to events irrespective of distance from camera and utilize the training outliers to determine the anomaly threshold.
- 2) We expand our analysis to nine participants with dementia and three different cameras.
- 3) We integrate the proposed approach into three different existing anomaly detection methods, referred to as their depth variants. The effectiveness of the proposed approach is then evaluated by comparing the performance of the depth variants with the existing methods.
- 4) We conduct an ablation analysis to investigate the effectiveness of individual components of the proposed approach and effect of frame size and frame rate in detecting behaviours of risk in PwD.
- 5) We analyze the performance of the proposed approach for generalization across cameras, participant-specific and sex-specific behaviours of risk detection in PwD.

II. RELATED WORK

In this section, we present the existing work for detecting behaviours of risk in PwD using videos and handling false positives in VAD scenarios.

Behaviours of Risk Detection: The current approaches for detecting behaviours of risk in PwD use different types of modalities, including wearable devices [6], computer vision [4], [7], radio waves [8] and multimodal / ambient sensing [9]. As this work uses videos, further review only discusses the studies that either use videos alone or in combination with other sensors. Qiu et al. [9] proposed a multimodal information fusion model using various sensors, including pressure sensors, ultrasound sensors, infrared sensors, video cameras, and acoustic sensors. A layered classification architecture, consisting of a hierarchical hidden Markov model and a support vector machine, was employed. However, their results were based on mock-up data generated through simulation. Chikhaoui et al. [10] developed an ensemble learning classifier to detect agitation using data from a Kinect camera and an accelerometer. Ten participants were instructed to perform six different agitated and aggressive behaviours. However, the study did not specify whether the participants were healthy volunteers or PwD. Fook et al. [7] introduced a method employing a multi-layer architecture of a probabilistic classifier based on hidden markov model and a support vector machine classifier. However, the video data involved a person in bed, and it was unclear whether the participants were healthy individuals

or PwD. For all the above studies, it appears that these systems were conceptual and were never tested with real patients, so their performance is unknown in a real-world setting. Acknowledging the importance of employing real-world data, in our previous work, we proposed an unsupervised convolutional autoencoder to detect agitation in PwD using videos collected from a specialized dementia unit from a single participant and a single camera [11]. In our later work [4] with the same limited dataset, we presented privacy-protecting VAD approaches to detect behaviours of risk in PwD using body pose information for the participants or semantic segmentation masks.

Video Anomaly Detection: VAD is a task in computer vision, aimed at identifying unusual or anomalous events in video sequences in the absence of anomalous samples during training. Among these, autoencoders and depth-based methods have emerged as prominent approaches. Liu et al. [12] proposed an appearance-motion united autoencoder framework for VAD which learned the appearance and motion normality jointly. Le and Kim [13] proposed an attention-based residual autoencoder which encoded both spatial and temporal information in a unified way. Schneider et al. [14] used foreground-aware loss and investigated how existing algorithms could leverage depth modality from Kinect camera to enhance detection performance. Denkovski et al. [15] proposed a multi-objective reconstruction and prediction-based loss to detect falls using multiple camera modalities including depth within a window of sequential frames.

Reducing False Positives: A VAD method can land into usability issues in the presence of increased false positives. Therefore, it is important to assess the rate of false positives (or false alarms) in these applications. We briefly review existing methods that handle false positives for VAD scenarios. Doshi and Yilmaz [16] proposed an online VAD method and a procedure for selecting an operating threshold that satisfied a desired false alarm rate. The framework was composed of deep learning-based feature extraction from video frames and a statistical sequential anomaly detection algorithm. Zhou et al. [17] proposed an anomaly trajectory detection framework for online traffic incident alerts on freeways. It used an adversarial loss to enable the autoencoder to learn a better normal trajectory pattern that is beneficial for reducing false alerts, while an abnormal trajectory discriminator was established and trained to detect small mean shifts and filter out instantaneous false alerts. Mozaffari et al. [18] proposed an online and multivariate anomaly detection method that was suitable for the timely and accurate detection of anomalies. They analyzed an asymptotic false alarm rate and provided a procedure for selecting a threshold to satisfy a desired false alarm rate. Singh et al. [19] aimed to address the challenge of a high false alarm rate resulting from the trade-off between learning to reconstruct and distinguish anomalies. They proposed a constrained generative adversarial network where white gaussian noise was added to the input to boost the robustness of the model.

The existing methods tried to reduce false positives by leveraging algorithmic designs or choosing the threshold depending on a desired false positive rate. However, as described in Section I, the sensitivity to the distance of objects/people

from the camera can be a determinant factor in the increased false positives in VAD tasks, especially for scenes with large variations in depth, such as corridors or hallways. Hence, we utilize the depth of pixels to handle this issue and enforce equivalent importance to events happening far and close to the camera, thus reducing the false positives.

III. METHODS

A. Data Collection

The video data used in this work was collected as part of a larger multimodal sensor study [6], [20] at the Specialized Dementia Unit (SDU) at Toronto Rehabilitation Institute, University Health Network (UHN), Toronto, Canada, between November 2017 and October 2019. The participants were admitted to the SDU from long-term care homes for the evaluation and management of behavioural and psychological symptoms in advanced dementia. Inclusion criteria encompassed individuals aged over 55 years, diagnosed with dementia and with a history of agitation or aggressive behaviours. The participants who expressed dissent to use of a wearable device (one of the study sensors, not part of this video-based study) were excluded from the study. Data collection ceased under either of the following circumstances: absence of documented agitation for one week, repeated removal of the wearable device, sickness, death or discharge from the unit, or upon completion of two months of data collection. The data collection was approved by the research ethics board (UHN REB#14-8483). Informed consent was obtained from substitute decision-makers for all participants. The staff also provided written consent for video recording within the unit. Additionally, all staff and decision-makers of participants shown in the images in the paper have granted written consent for the publication of their images.

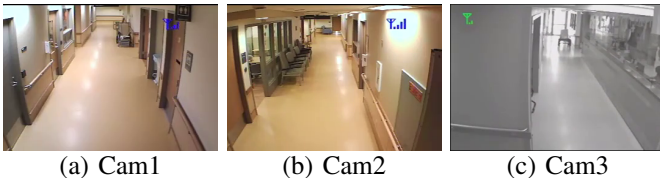


Fig. 1: Three different installed camera views.

TABLE I: Participants’ demographic information.

Attribute	Value
Number of Participants	9
Median age of participants (years)	82
Mean age of participants (years)	81.22
Standard deviation of the age of participants (years)	8.12
Range of age of participants (years)	66–93
Gender	Males (3) Females (6)

B. Selected Dataset

For this study, we selected a subset of videos, approximately 93.5 hours for each camera, based on 30 minutes before and after each documented behaviour of risk event from the

larger video dataset comprising the top three cameras (see Fig. 1). Table I presents the demographic information of the participants. The selected video data captured the behaviours of risk events for nine dementia participants with an age range of 66–93 years and a mean age of 81.22 ± 8.12 years. There were three male and six female participants.

C. Data Annotation

Two research assistants were hired on a part-time basis and independently reviewed selected videos containing behaviour of risk events across Cam1, 2 and 3. We had the timestamps of each behaviour of risk event, so the annotators did not have to watch the entire video feed but only look at the selected segment for each behaviour of risk event. This activity took approximately two months and they annotated all the events corresponding to motor or physical agitation. Due to the lack of audio during data collection, it was not possible to annotate verbal aggression. Anvil [21] tool was used for the annotation of camera videos. Both the research assistants annotated the videos separately for the presence of behaviours of risk events and other activities, namely, the presence of unusual activities, crowded scenes and large objects. The two assistants individually annotated 305 and 383 behaviours of risk events across three cameras and nine participants. For the final labelling, an event was labelled as behaviour of risk if either of the research assistants annotated it as a behaviour of risk. For cases where both the assistants annotated an event as behaviour of risk but disagreed in the start/end times of the annotation, the duration with common agreement was labelled as a behaviour of risk. An inter-rater agreement analysis was performed, where Cohen’s kappa [22], Krippendorff alpha [23] and percentage agreement metrics were calculated over the annotations of both research assistants. The metrics were calculated based on the timestamps (in seconds) of the annotations of the two annotators. This was done to measure the agreeability of the two annotations over the categorization of the events into normal and behaviours of risk events. The Cohen’s kappa, Krippendorff alpha and percentage agreement were determined as 0.48, 0.48 and 0.99, respectively. The value of Cohen’s kappa and Krippendorff alpha can range from -1 to 1 , where 1 and -1 represent a perfect agreement and disagreement, and 0 represents agreement expected from random chance.

D. Data Preprocessing

The original resolution, frame rate and bit depth of the videos were 352×240 , 30 frames per second (fps) and 24, respectively. The frames were sampled from the videos at 15 fps, selecting every second frame. The frames were then converted to grayscale, normalized to range $[0, 1]$ (pixel values divided by 255) and resized to 64×64 resolution using the python programming language. This was done to minimize the computational expenses associated with trainable parameters. The frames were then stacked separately to form non-overlapping 5-second windows (75 frames per window) (based on previous work [11]). The labels for behaviours of risk were refined in accordance with the 5-second windows. Training and

TABLE II: Size of training and test sets (in minutes).

	Cam1	Cam2	Cam3
Train set	1225.25	1242.33	1205.66
Test set	209.16	291.92	96
Normal behaviour (Test set)	194.08	270.5	89.83
Behaviours of risk (Test set)	15.08	21.42	6.17

TABLE III: Number of 5-second windows and types of behaviours of risk across participants and cameras in test set.

Participant-ID	Sex	Cam1	Cam2	Cam3	Type of behaviour of risk
Participant1	F	17	25	12	Hitting, Pushing, Falling, Kicking, Grabbing, Throwing, Other
Participant2	F	3	3	1	Pushing, Other
Participant3	M	15	26	15	Hitting, Pushing, Kicking, Grabbing, Other
Participant4	F	121	199	44	Hitting, Pushing, Kicking, Grabbing, Throwing, Other
Participant5	F	0	0	1	Hitting, Pushing, Kicking, Other
Participant6	M	17	0	1	Hitting, Pushing, Kicking, Grabbing, Other
Participant7	F	8	0	0	Pushing, Grabbing, Other
Participant8	F	0	3	0	Pushing, Other
Participant9	M	0	1	0	Hitting, Grabbing, Other

test sets were generated individually for the three cameras. The training sets were composed of normal behaviours from daily activities only. The test sets were composed of both normal and behaviours of risk events. The training set size was fixed around an average of 1224.41 minutes across three cameras. The test set consists of a combination of behaviours of risk events from nine participants across three cameras along with normal behaviours. In the test sets, the available duration of annotated behaviours of risk events was limited. Hence, the duration of normal behaviour in test sets was chosen to keep a similar imbalance ratio (as in previous work [4]), which is approximately 7% for behaviours of risk events. Table II shows the size of training and test sets for each of the three cameras. The test set was used to evaluate the performance of methods for detecting behaviours of risk. The number of 5-second windows and types of behaviours of risk across participants and cameras in the test set are presented in Table III.

E. Behaviours of Risk Detection

In our previous work [4], [11], we used a customized spatio-temporal convolutional autoencoder (3DCAE) to detect behaviours of risk from data from one participant and a single camera. 3DCAE learned to reconstruct the input videos with normal behaviour during training. Hence, during testing, normal instances were expected to have a lower reconstruction error, while instances with high reconstruction error were treated as anomalies (behaviours of risk in our case). However, it showed high false positives due to sensitivity to activities such as crowded scenes, large objects, or other events happening near the camera due to reasons described in Section I. Such instances are extremely common in normal day-to-day activities happening in care units. As such, there was a need to handle this issue to make the method suitable for real-world deployment. Hence in this work, we propose a novel depth-weighted loss, where the depth of the pixels is used as a weight

factor to enforce equivalent importance to both behaviours of risk and non-behaviours of risk events happening far and near the camera. It is hypothesized that the weighted-depth loss will lead to a reduction in false positives in this problem. We also propose a new way to determine the threshold for detecting behaviours of risk as anomalies using the abnormal non-behaviours of risk activities in the training set as outliers. Hence, the proposed approach consists of the novel depth-weighted loss and utilizing the training outliers to determine the threshold.

Depth-weighted Anomaly Score: Existing autoencoder methods [4] employ reconstruction error to detect anomalous frames. This strategy inherently favours anomalies closer to the camera, as they occupy more pixels in the image plane. This bias poses a challenge, especially in scenes with highly varying distances from the camera, such as corridors (see Fig. 1). As a result, anomalies at different distances receive unequal anomaly scores, with those closer to the camera being unfairly favoured. To address this problem, we propose a loss where depth per pixel is used as weight during the calculation of reconstruction error to enforce equivalent importance to both near and far pixels.

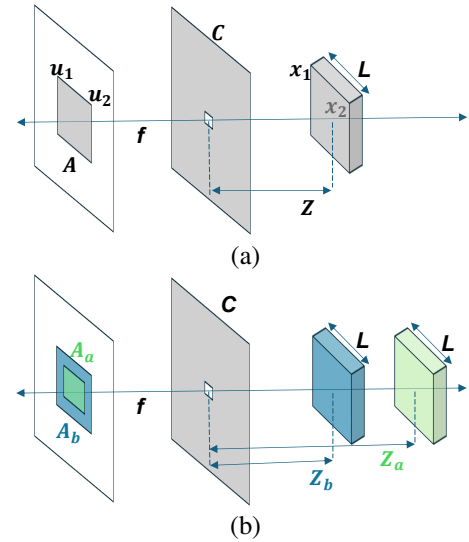


Fig. 2: (a) Illustration of the geometric relationship between a 3D prism (side length L) and the area of its projection in the image plane. (b) Two identical 3D prisms placed at different distances from camera position C ($Z_a > Z_b$) produce a smaller projected area ($A_a < A_b$).

To understand the translation of an anomaly in 3D space, we describe the relationship between the area A depicting the anomaly in the image plane and its 3D volume. For simplicity, we consider this 3D volume as a square prism (see Fig. 2 (a)). Consider two of the vertex of the square prism represented as $x_1 = (X_1, Y_1, Z_1)$ and $x_2 = (X_2, Y_2, Z_2)$ in the 3D space and their 2D projections $u_1 = (U_1, V_1)$ and $u_2 = (U_2, V_2)$ in the image plane. In Fig. 2, C refers to the camera position. The projection of a 3D point (X, Y, Z) onto a 2D image plane is expressed by the image coordinates (U, V) through the pinhole camera model [24] equations as,

$$U = \frac{fX}{Z}, \quad V = \frac{fY}{Z} \quad (1)$$

where f is the focal length and Z is the distance from the 3D object to the camera position. Assuming the difference in depth Z between these vertices is negligible ($Z \approx Z_1 \approx Z_2$), the projections on the image plane according to equation (1) are:

$$U_1 = \frac{fX_1}{Z}, \quad U_2 = \frac{fX_2}{Z} \quad (2)$$

Given that the length between the vertices in the 3D space along the X-axis is $L = |X_2 - X_1|$, the area A of the square in the 2D plane containing the anomaly is:

$$A = (U_2 - U_1)^2 = \left(\frac{f}{Z}\right)^2 (X_2 - X_1)^2 = \left(\frac{fL}{Z}\right)^2 \quad (3)$$

To analyze the sensitivity of the anomaly score (AS) on the distance from the camera and therefore, on the area in the image plane, we can express the anomaly score of an area A as,

$$AS_A = \overline{AS}_{\text{pixel}} \cdot A \quad (4)$$

where $\overline{AS}_{\text{pixel}}$ represents the average anomaly score per pixel, a constant value that depends solely on the anomaly itself, irrespective of its position in 3D space or its projection onto the image plane.

Consider an anomaly event occurring at different distances Z_a and Z_b from the camera. As it is the same event with same volume, it will have same value of $\overline{AS}_{\text{pixel}}$ and length L at both distances. As illustrated in Fig. 2 (b), when projected in the image plane, this results in different area values A_a and A_b in the image plane, with $A_a < A_b$ if $Z_a > Z_b$. Since both anomalies have the same value of $\overline{AS}_{\text{pixel}}$, according to equation (4), the difference in area will result in a different anomaly score. To ensure depth invariance, we need the anomaly to have the same score AS_{inv} regardless of its distance from the camera. This is achieved by introducing a factor K :

$$AS_{inv} = K_a \cdot AS_{A_a} = K_b \cdot AS_{A_b} \quad (5)$$

Combining the equations (3), (4) and (5), we can express AS_{inv} as :

$$AS_{inv} = K_a \overline{AS}_{\text{pixel}} (fL)^2 \frac{1}{Z_a^2} = K_b \overline{AS}_{\text{pixel}} (fL)^2 \frac{1}{Z_b^2} \quad (6)$$

Therefore, given the constant value of $\overline{AS}_{\text{pixel}}$ and $(fL)^2$, to achieve depth invariance, the factors K_a and K_b must satisfy the following conditions:

$$K_a = Z_a^2, \quad K_b = Z_b^2 \quad (7)$$

Based on this, we propose the following novel loss where depth per pixel is used as weight during the calculation of reconstruction error as mean squared error to enable the

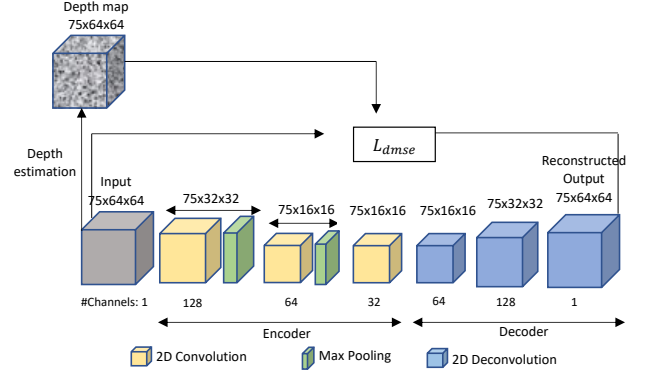


Fig. 3: depCAE architecture to detect behaviours of risk.

methods to enforce equivalent importance to both near and far pixels.

$$L_{dmse} = \frac{1}{N_e} \sum_{l=1}^W \sum_{i=1}^S \sum_{j=1}^S \phi_{l,i,j} (I_{l,i,j} - O_{l,i,j})^2 \quad (8)$$

where, I is the input pixel, O is the reconstructed pixel, S is the spatial size, and W represents the number of frames in a window. $N_e = W \times S \times S$ is the total number of pixels in a window. The depth-based weight hyperparameter ϕ can be expressed as a function of Z^2 , i.e., $\phi = f(Z^2)$. The value of ϕ is chosen using cross-validation from among different functions of Z^2 , namely $(Z^2, Z^2/2, \sqrt{Z^2} = Z)$, by leveraging the proxy validation set in a similar way as the threshold. The weighted-depth loss helped the method to treat both the near and far behaviours of risk events with similar importance, which in turn helped to reduce false positives. The dense prediction transformer [25] was used to estimate the depth map during both training and testing. During testing, the depth-weighted loss was used as anomaly score for detecting behaviours of risk.

Threshold Determination: In an anomaly detection approach, it can be challenging to determine an operating threshold due to the absence of anomalous samples in the training set. As discussed in Section III-C, the data was annotated for other unusual activities, such as large objects, crowded scenes and other infrequent activities in the training set. Due to the unusual nature of these annotated activities relative to the activities of daily living in a dementia unit, we propose to treat these activities as proxy outliers to create a proxy validation set to determine the threshold. Following a similar approach as in our previous work [26], we chose each reconstruction error as a threshold during training and found the corresponding F1-score on the proxy validation set. Finally, the reconstruction error with the highest F1-score was chosen as the operating threshold. The operating threshold was then utilized during testing to detect behaviours of risk in the test set and the results were reported in Section IV.

Experimental Setup: Transformers and variational autoencoders have performed well in the existing literature for VAD [27], [28]. In this work, we have used three different anomaly detection methods, namely, 3DCAE, a self-supervised masked

convolutional transformer block-based autoencoder (CTBAE) and a variational autoencoder (VAE) for evaluation. The 3DCAE method has been adapted from our previous work [4]. The CTBAE method used a self-supervised masked convolutional transformer block [27] embedded after the encoder layer and its output was passed as input to the decoder. VAE [29] learned to generate two vectors that represent the parameters (mean and variance) of a distribution from which the latent vector was sampled. For fairness during comparison, the encoder and decoder architecture of 3DCAE, CTBAE and VAE were kept the same and they used interquartile range (IQR) generated proxy-validation set [26] for threshold calculation. The proposed depth-weighted approach was integrated as part of the 3DCAE, CTBAE and VAE methods and their depth variants are referred to as depCAE, depCTBAE and depVAE, respectively. The depCAE method followed an encoder-decoder architecture, where the encoder consisted of 2D convolution and max-pooling layers, with a kernel size of $(1 \times 3 \times 3)$, stride $(1 \times 1 \times 1)$ and padding $(0 \times 1 \times 1)$, followed by batch normalization and ReLU operations. The decoder used 2D deconvolution layers (2D transposed convolution operation) with a kernel size of $(1 \times 3 \times 3)$, strides $(1 \times 1 \times 1)$, $(1 \times 2 \times 2)$, $(1 \times 2 \times 2)$ and paddings $(0 \times 1 \times 1)$, $(0 \times 1 \times 1)$, $(0 \times 1 \times 1)$ for first, second, and third 2D deconvolution layers, respectively. The overall architecture of the depCAE is presented in Fig. 3. In the depCAE method, $W = 75$ and $N_e = 75 \times 64 \times 64 = 307200$.

Evaluation Metrics: The proposed approach aims to reduce false positives; however, it is also important to consider false negatives when detecting behaviours of risk in PwD. Hence, when evaluating performance, it is important to consider a metric that can give a balanced estimate of the performance on both false positive rate (FPR) and false negative rate (FNR). Precision and recall can be expressed as,

$$Precision = \frac{TPR}{TPR + \frac{1}{\gamma}FPR} \quad (9)$$

$$Recall = \frac{TPR}{TPR + FNR} \quad (10)$$

where TPR refers to true positive rate and $\gamma = \frac{No. of positives (P)}{No. of negatives (N)}$ is class ratio. As seen in eqns. 9 and 10, precision and recall give an estimate of the performance over FPR and FNR, respectively. F1-score is the harmonic mean of precision and recall, and provides a reasonable performance estimate over TPR, FPR and FNR, simultaneously. Matthew's Correlation Coefficient (MCC) gives an overall performance estimate over true positives (TP), true negatives (TN), false positives (FP) and false negatives (FN) and is expressed as,

$$MCC = \frac{TP * TN - FP * FN}{\sqrt{(TP + FP) * P * N * (TN + FN)}} \quad (11)$$

Both F1-score and MCC are threshold-based metrics; hence they evaluate performance over a single threshold. The area under the curve of receiver operating characteristic (AUROC) evaluates the performance over TPR and FPR over a range of thresholds. Hence, the primary metrics employed for evaluating the performance of methods in this work are MCC,

F1-score and AUROC. We also report additional metrics for reference, namely, TPR, true negative rate (TNR), FPR, FNR, $gmean(\sqrt{TPR * TNR})$, precision, recall, specificity, and balanced accuracy [30]. The evaluation metrics use reconstruction error as the score to identify behaviours of risk as anomalies during testing.

TABLE IV: Performance comparison of depth variants and existing methods for Cam1.

	Existing methods			Depth variants		
	3DCAE	CTBAE	VAE	depCAE	depCTBAE	depVAE
TPR	0.945	0.950	0.641	0.939	0.773	0.552
TNR	0.628	0.581	0.713	0.684	0.742	0.780
FPR	0.372	0.419	0.287	0.316	0.258	0.220
FNR	0.055	0.050	0.359	0.061	0.227	0.448
Gmean	0.770	0.743	0.676	0.801	0.758	0.657
Precision	0.165	0.150	0.148	0.187	0.189	0.163
Recall	0.945	0.950	0.641	0.939	0.773	0.552
Specificity	0.628	0.581	0.713	0.684	0.742	0.780
Balanced Accuracy	0.786	0.765	0.677	0.811	0.758	0.666
MCC	0.301	0.276	0.198	0.335	0.293	0.200
F1-score	0.281	0.259	0.240	0.313	0.304	0.252
AUROC	0.844	0.779	0.754	0.852	0.823	0.784

TABLE V: Performance comparison of depth variants and existing methods for Cam2.

	Existing methods			Depth variants		
	3DCAE	CTBAE	VAE	depCAE	depCTBAE	depVAE
TPR	0.949	0.728	0.502	0.844	0.412	0.751
TNR	0.611	0.668	0.812	0.686	0.832	0.719
FPR	0.389	0.332	0.188	0.314	0.168	0.281
FNR	0.051	0.272	0.498	0.156	0.588	0.249
Gmean	0.761	0.697	0.638	0.761	0.586	0.735
Precision	0.162	0.148	0.174	0.176	0.163	0.175
Recall	0.949	0.728	0.502	0.844	0.412	0.751
Specificity	0.611	0.668	0.812	0.686	0.832	0.719
Balanced Accuracy	0.780	0.698	0.657	0.765	0.622	0.735
MCC	0.290	0.215	0.200	0.290	0.164	0.264
F1-score	0.276	0.246	0.259	0.291	0.234	0.284
AUROC	0.810	0.766	0.790	0.810	0.757	0.792

TABLE VI: Performance comparison of depth variants and existing methods for Cam3.

	Existing methods			Depth variants		
	3DCAE	CTBAE	VAE	depCAE	depCTBAE	depVAE
TPR	0.919	0.649	0.230	0.730	0.743	0.135
TNR	0.530	0.645	0.903	0.714	0.622	0.931
FPR	0.470	0.355	0.097	0.286	0.378	0.069
FNR	0.081	0.351	0.770	0.270	0.257	0.865
Gmean	0.698	0.647	0.455	0.722	0.680	0.355
Precision	0.118	0.111	0.139	0.149	0.119	0.119
Recall	0.919	0.649	0.230	0.730	0.743	0.135
Specificity	0.530	0.645	0.903	0.714	0.622	0.931
Balanced Accuracy	0.724	0.647	0.566	0.722	0.682	0.533
MCC	0.220	0.149	0.105	0.235	0.182	0.063
F1-score	0.210	0.190	0.173	0.248	0.205	0.127
AUROC	0.765	0.739	0.709	0.768	0.722	0.696

IV. RESULTS AND DISCUSSION

In this section, we evaluate the performance of the proposed approach for FP reduction and detecting behaviours of risk in PwD. We conduct an ablation analysis of different components of the proposed approach and the effect of frame size and

frame rate on the performance of detecting behaviours of risk. We further perform cross-camera, participant and sex-specific analysis.

Performance Evaluation: We investigate the effectiveness of the proposed approach for reducing FP and detecting behaviours of risk by evaluating the improvement in performance after integrating the proposed approach into existing methods. As discussed in Section III-E, depth variants were created after integrating the proposed approach into the existing methods. Tables IV, V and VI compare the performance of the depth variants with their existing method counterparts for behaviours of risk detection for Cam1, Cam2 and Cam3, respectively. The best values for FPR and primary evaluation metrics, MCC, F1-score and AUROC, are marked in bold. It can be observed that depCAE performed mostly better than 3DCAE in terms of MCC, F1-score and AUROC for all three cameras. depCTBAE performed better than CTBAE for Cam1 and Cam3, while depVAE performed better than VAE for Cam1 and Cam2. depCAE recorded lower FPR than 3DCAE for all three cameras. depCTBAE and depVAE recorded lower FPR than CTBAE and VAE, respectively, for two out of three cameras. The methods performed better for Cam1 and Cam2 in comparison to Cam3, which can be attributed to the major portion of Cam3 view being occluded by the wall. This made it difficult to gauge the behaviours of risk events clearly in Cam3. For the case of secondary evaluation metrics, gmean, precision and specificity, the depth variants mostly performed better than the existing methods across the three cameras. The depCAE method achieved the best MCC, F1-score and AUROC overall for all three cameras; hence further analysis in this section is performed using depCAE method. The depCAE method achieved a MCC, F1-score and AUROC of 0.335, 0.313, 0.852 for Cam1, 0.29, 0.291, 0.81 for Cam2, and 0.235, 0.248, 0.768 for Cam3, respectively. While depVAE gave lower FPR as compared to other methods, it gave significantly higher FNR. In such cases, it is important to consider a balanced evaluation over both FPR and FNR, which is provided by F1-score, where depCAE performed the best. It can be inferred from the observations that the proposed approach of weighing the loss with pixel depth is indeed effective in reducing false positives and improving detection performance. Further, the proposed approach can be easily integrated into any existing autoencoder-based anomaly detection method.

Ablation Analysis I (Relative Effectiveness of the Proposed Components): We investigate the relative effectiveness of the two components of the proposed method, namely, depth-weighted loss and threshold determination using annotated outliers, in detecting behaviours of risk in PwD. Table VII presents the results for ablation analysis over three cameras, where depWgtOnly refers to the setting of depCAE trained using depth-weighted loss while using IQR outliers [26] for threshold calculation, and anntThrOnly refers to the setting of using mean squared error loss while using annotated outliers for threshold calculation. The best MCC, F1 scores and AUROC are marked in bold. For Cam1, anntThrOnly performed better than depWgtOnly in terms of MCC and F1-score, while depWgtOnly performed better in terms of AUROC. Overall, depCAE benefited from the combined performance

of depWgtOnly and anntThrOnly giving an AUROC of 0.852. For Cam2, anntThrOnly performed similar to depCAE in terms of AUROC, while the performance of depCAE degraded in comparison to anntThrOnly in terms of MCC and F1-score. For Cam3, depCAE benefited from the combined functionality of depWgtOnly and anntThrOnly, outperforming both of them in terms of MCC, F1-score and AUROC. Overall, it can be observed that both depWgtOnly and anntThrOnly are vital components of depCAE and contribute significantly towards the performance of depCAE.

Ablation Analysis II (Effect of Frame Size and Frame Rate): We investigate the effect of increasing the frame size and decreasing the frame rate in detecting behaviours of risk in PwD. Table VIII presents the results for ablation analysis over three cameras, where s64r15 refers to the original 64×64 frame size and 15 fps setting, and s128r8 refers to 128×128 frame size and 8 fps setting. For s128r8, a lower frame rate was used to manage the computation complexity added due to increase in frame size. The best MCC, F1 score and AUROC are marked in bold. It was observed that for Cam1, s128r8 performed better than s64r15 in terms of MCC and F1-score, while s64r15 performed better in terms of AUROC. For Cam2 and Cam3, s64r15 performed better in terms of all of MCC, F1-score and AUROC metrics. Overall, it was observed that s64r15 performed similar or better than s128r8. Increasing the frame size did not lead to any significant improvement in performance. The depCAE method can extract the necessary information for detecting behaviours of risk from a low resolution of 64×64 , which may be difficult for the human eye.

Cross-Camera Analysis: We investigate the performance of depCAE to detect behaviours of risk in a new camera that was not seen during training. As part of this analysis, the depCAE method was trained on Cam2 and tested on Cam1 and vice-versa, as seen in Table IX. The results are compared with the setting where the method is trained and tested on the same camera. It was observed that there was a drop in performance when the method was trained on a camera different from the testing camera. A drop in F1-score performance of 0.041 (0.313-0.272) and 0.052 (0.291-0.239), and in AUROC performance of 0.056 (0.852-0.796) and 0.04 (0.81-0.77) was observed when the method was tested on Cam1 and Cam2, respectively. The performance drop was expected and within reasonable limits as the training camera was different from the testing camera and no fine-tuning was involved. We have discussed some strategies to improve the cross-camera performance in Section V as part of our future work.

Participant-Specific Analysis: As presented in Table III, the type of behaviours of risk varied across participants. Hence, it is crucial to consider the potential dissimilar performance across individuals when training and testing behaviours of risk detection methods. Table X presents the performance of depCAE separately for each participant involved in the study across three cameras. “-” represents the cases where one or less than one agitation window was recorded for the participants. In general, it can be observed that depCAE showed better behaviours of risk detection performance for participants

TABLE VII: Ablation analysis of proposed components of depCAE across three different cameras.

Metric	Cam1			Cam2			Cam3		
	depWgtOnly	anntThrOnly	depCAE	depWgtOnly	anntThrOnly	depCAE	depWgtOnly	anntThrOnly	depCAE
Gmean	0.760	0.805	0.801	0.743	0.791	0.761	0.624	0.647	0.722
Precision	0.158	0.202	0.187	0.158	0.188	0.176	0.098	0.135	0.149
Recall	0.967	0.895	0.939	0.879	0.907	0.844	0.905	0.554	0.730
Specificity	0.598	0.725	0.684	0.628	0.690	0.686	0.430	0.756	0.714
Balanced Accuracy	0.782	0.81	0.811	0.754	0.798	0.765	0.668	0.655	0.722
MCC	0.294	0.344	0.335	0.269	0.325	0.290	0.167	0.172	0.235
F1-score	0.271	0.32	0.313	0.267	0.311	0.291	0.177	0.217	0.248
AUROC	0.851	0.842	0.852	0.802	0.81	0.81	0.765	0.768	0.768

TABLE VIII: Ablation analysis of input frame size and frame rates for depCAE.

Metric	Cam1		Cam2		Cam3	
	s64r15	s128r8	s64r15	s128r8	s64r15	s128r8
Gmean	0.801	0.808	0.761	0.645	0.722	0.653
Precision	0.187	0.199	0.176	0.198	0.149	0.105
Recall	0.939	0.917	0.844	0.494	0.730	0.851
Specificity	0.684	0.712	0.686	0.841	0.714	0.501
Balanced Accuracy	0.811	0.815	0.765	0.668	0.722	0.676
MCC	0.335	0.345	0.290	0.226	0.235	0.173
F1-score	0.313	0.326	0.291	0.282	0.248	0.187
AUROC	0.852	0.848	0.810	0.795	0.768	0.739

TABLE IX: Cross-camera analysis for depCAE.

	Train-test on Cam1	Train on Cam2 test on Cam1	Train-test on Cam2	Train on Cam1 test on Cam2
Gmean	0.801	0.750	0.761	0.704
Precision	0.187	0.162	0.176	0.139
Recall	0.939	0.862	0.844	0.848
Specificity	0.684	0.653	0.686	0.585
Balanced Accuracy	0.811	0.757	0.765	0.717
MCC	0.335	0.274	0.290	0.227
F1-score	0.313	0.272	0.291	0.239
AUROC	0.852	0.796	0.810	0.770

showing less diverse episodes of behaviours of risk, namely, participants 2, 7 and 8, as compared to participants with more diverse episodes. depCAE performed generally well for participant 3 across cameras 1 and 2 and across all three cameras for participant 4, for whom the most number of behaviours of risk windows were recorded. On average, the detection performance was better for participants on cameras 1 and 2 as compared to camera 3.

Sex-Specific Analysis: It is important to investigate the performance of depCAE across population groups. Table XI presents the performance of depCAE stratified based on sex across three cameras. As can be seen in Table III, some participants did not show any behaviours of risk event in one or two cameras, leading to the situation with only 6 participants with differing participant ids for any individual camera. However, the overall sex-specific analysis was done for all 9 participants. A similar behaviour of risk detection performance was observed for both males and females for Cam1. However, for cameras 2 and 3 it was observed that the depCAE method performed better for females than males. The reason for this can be attributed to the presence of more females than males in the study, leading to the skewed class distribution due to the presence of more behaviours of risk windows for females than males, enhancing the method's

TABLE X: depCAE performance stratified over participants.

	Cam1		Cam2		Cam3	
	F1-score	AUROC	F1-score	AUROC	F1-score	AUROC
Participant1	0.239	0.695	0.226	0.669	0.277	0.804
Participant2	0.3	0.895	0.75	0.964	-	-
Participant3	0.345	0.905	0.265	0.742	0.178	0.635
Participant4	0.324	0.878	0.307	0.832	0.274	0.806
Participant5	-	-	-	-	-	-
Participant6	0.276	0.784	-	-	-	-
Participant7	0.32	0.819	-	-	-	-
Participant8	-	-	0.375	0.856	-	-
Participant9	-	-	-	-	-	-
Average	0.3	0.829	0.385	0.813	0.243	0.748

TABLE XI: depCAE performance stratified over sex.

	Cam1		Cam2		Cam3	
	F1-score	AUROC	F1-score	AUROC	F1-score	AUROC
Male (N=2)	0.310	0.837	0.266	0.738	0.160	0.637
Female (N=4)	0.313	0.856	0.294	0.817	0.276	0.806

learning and generalization capabilities for females.

While the study presented important findings for the detection of behaviours of risk in PwD over multiple participants and cameras, there are some limitations associated with the study. First, as the SDU, where the data collection was conducted, usually admits PwD with severe cases of behavioural and psychological symptoms, the number of behaviours of risk episodes displayed by PwD can be higher than a standard LTC facility. Hence, it is crucial to revalidate these findings on the data collected in LTC facilities where the frequency of behaviours of risk episodes is expected to be lower. Second, due to privacy reasons, no camera was installed in private rooms, limiting the analysis of behaviours of risk episodes in public hallways. Hence, the applicability of our findings to more private settings remains unclear. Despite these limitations, our approach effectively detects behaviours of risk episodes with the best AUROC of 0.852, establishing it as the preferred option over existing methods.

V. CONCLUSION AND FUTURE WORK

Caring for individuals with dementia in care settings is increasingly challenging due to growing patient numbers and understaffing issues. The behavioural and psychological symptoms of dementia can lead to incidents that jeopardize the health and safety of patients, staff, and caregivers. Leveraging existing video infrastructure can enable the development of innovative deep-learning approaches to detect such behaviours, thereby preventing injuries and enhancing patient care. As a step in this direction, we proposed an approach that uses a

novel depth-weighted loss to enforce equivalent importance to both near and far events and uses training outliers to determine the anomaly threshold. The depCAE achieved AUROC of 0.852, 0.81 and 0.768 for the three cameras, outperforming other methods. The proposed approach recorded lower FPR than the existing methods across all three cameras, thus reducing the false alarms in detecting behaviours of risk in PwD. Further, the proposed approach consistently demonstrated its effectiveness and can easily be integrated into any existing autoencoder-based anomaly detection method. This motivates further multidisciplinary research for the deployment of video surveillance-based behaviours of risk detection systems in nursing and care settings for PwD. Similar multidisciplinary approaches have shown to be helpful in medical settings [31], [32]. A video-based behaviours of risk detection system will help to improve the quality of life for the residents in care homes.

Future work can involve validating our approach on data collected from an LTC that typically encounters fewer behaviours of risk incidents. The influence of camera placement on the global system performance needs to be further investigated by evaluating how the position, angle, and orientation of the cameras impact the system's ability to accurately and reliably detect behaviours of risk. Further, the effect of utilizing the depth map as part of data as an additional input channel can be investigated. 3D object reconstruction-based approaches [33], [34] can be used to circumvent the problem of occlusions and improve the performance of detecting behaviours of risk as anomalies. Pose tracking cameras that directly extract body joints information without recording actual scene [35] can be employed in private areas to detect behaviours of risk in a privacy-protecting manner [4], [36]. It can be a time-consuming and expensive task to train a method separately on each new scene or environment. A lot of time and resources can be saved if a method trained on one scene can generalize well in detecting behaviours of risk in an entirely new scene. Fine-tuning on target camera using few-shot learning and transfer learning can be employed to improve the performance of depCAE for cross-camera generalization.

In conclusion, this work marks an important step for the development of an automated behaviours of risk detection system that can be employed in real-world care settings and helps to improve the care and safety of PwD in assisted living facilities.

REFERENCES

- [1] J. Cohen-Mansfield, "Instruction manual for the cohen-mansfield agitation inventory (cmai)," *Research Institute of the Hebrew Home of Greater Washington*, vol. 1991, 1991.
- [2] M. of Long-Term Care, "Long-term care staffing study," July 202, <https://www.ontario.ca/page/long-term-care-staffing-study> [Online; accessed 1-March-2023].
- [3] P. K. Mishra, C. Gautam, and A. Tiwari, "Minimum variance embedded auto-associative kernel extreme learning machine for one-class classification," *Neural Computing and Applications*, vol. 33, no. 19, pp. 12973–12987, 2021.
- [4] P. K. Mishra, A. Iaboni, B. Ye, K. Newman, A. Mihailidis, and S. S. Khan, "Privacy-protecting behaviours of risk detection in people with dementia using videos," *BioMedical Engineering OnLine*, vol. 22, no. 1, pp. 1–17, 2023.
- [5] K. Liu and H. Ma, "Exploring background-bias for anomaly detection in surveillance videos," in *Proceedings of the 27th ACM International Conference on Multimedia*, 2019, pp. 1490–1499.
- [6] S. Spasojevic, J. Nogas, A. Iaboni, B. Ye, A. Mihailidis, A. Wang, S. J. Li, L. S. Martin, K. Newman, and S. S. Khan, "A pilot study to detect agitation in people living with dementia using multi-modal sensors," *Journal of Healthcare Informatics Research*, vol. 5, no. 3, pp. 342–358, 2021.
- [7] V. F. S. Fook, P. V. Thang, T. M. Htwe, Q. Qiang, A. A. P. Wai, M. Jayachandran, J. Biswas, and P. Yap, "Automated recognition of complex agitation behavior of dementia patients using video camera," in *2007 9th International Conference on e-Health Networking, Application and Services*. IEEE, 2007, pp. 68–73.
- [8] N. Sharma, J. Klein Brinke, L. Braakman Jansen, P. J. Havinga, and D. V. Le, "Wi-gitation: Replica wi-fi csi dataset for physical agitation activity recognition," *Data*, vol. 9, no. 1, p. 9, 2023.
- [9] Q. Qiu, S. F. Foo, A. A. P. Wai, V. T. Pham, J. Maniyeri, J. Biswas, and P. Yap, "Multimodal information fusion for automated recognition of complex agitation behaviors of dementia patients," in *2007 10th International Conference on Information Fusion*. IEEE, 2007, pp. 1–8.
- [10] B. Chikhaoui, B. Ye, and A. Mihailidis, "Ensemble learning-based algorithms for aggressive and agitated behavior recognition," in *Ubiquitous Computing and Ambient Intelligence*. Cham: Springer International Publishing, 2016, pp. 9–20.
- [11] S. S. Khan, P. K. Mishra, N. Javed, B. Ye, K. Newman, A. Mihailidis, and A. Iaboni, "Unsupervised deep learning to detect agitation from videos in people with dementia," *IEEE Access*, vol. 10, pp. 10349–10358, 2022.
- [12] Y. Liu, J. Liu, J. Lin, M. Zhao, and L. Song, "Appearance-motion united auto-encoder framework for video anomaly detection," *IEEE Transactions on Circuits and Systems II: Express Briefs*, vol. 69, no. 5, pp. 2498–2502, 2022.
- [13] V.-T. Le and Y.-G. Kim, "Attention-based residual autoencoder for video anomaly detection," *Applied Intelligence*, vol. 53, no. 3, pp. 3240–3254, 2023.
- [14] P. Schneider, J. Rambach, B. Mirbach, and D. Stricker, "Unsupervised anomaly detection from time-of-flight depth images," in *Proceedings of the IEEE/CVF Conference on Computer Vision and Pattern Recognition*, 2022, pp. 231–240.
- [15] S. Denkovski, S. S. Khan, and A. Mihailidis, "Temporal shift-multi-objective loss function for improved anomaly fall detection," in *Asian Conference on Machine Learning*. PMLR, 2024, pp. 295–310.
- [16] K. Doshi and Y. Yilmaz, "Online anomaly detection in surveillance videos with asymptotic bound on false alarm rate," *Pattern Recognition*, vol. 114, p. 107865, 2021.
- [17] W. Zhou, Y. Yu, Y. Zhan, and C. Wang, "A vision-based abnormal trajectory detection framework for online traffic incident alert on freeways," *Neural Computing and Applications*, vol. 34, no. 17, pp. 14945–14958, 2022.
- [18] M. Mozaffari, K. Doshi, and Y. Yilmaz, "Self-supervised learning for online anomaly detection in high-dimensional data streams," *Electronics*, vol. 12, no. 9, p. 1971, 2023.
- [19] R. Singh, A. Sethi, K. Saini, S. Saurav, A. Tiwari, and S. Singh, "Cvadgan: Constrained video anomaly detection via generative adversarial network," *Image and Vision Computing*, vol. 143, p. 104950, 2024.
- [20] S. S. Khan, P. K. Mishra, B. Ye, S. Patel, K. Newman, A. Mihailidis, and A. Iaboni, "A novel multi-modal sensor dataset and benchmark to detect agitation in people living with dementia in a residential care setting," *researchgate.net*, 2024.
- [21] M. Kipp, *Multimedia Annotation, Querying, and Analysis in Awil*. John Wiley and Sons, Ltd, 2012, ch. 21, pp. 351–367.
- [22] M. L. McHugh, "Interrater reliability: the kappa statistic," *Biochemia Medica*, vol. 22, no. 3, pp. 276–282, 2012.
- [23] K. Krippendorff, "Estimating the reliability, systematic error and random error of interval data," *Educational and Psychological Measurement*, vol. 30, no. 1, pp. 61–70, 1970.
- [24] P. Sturm, "Pinhole camera model," in *Computer Vision: A Reference Guide*. Springer, 2021, pp. 983–986.
- [25] R. Ranftl, A. Bochkovskiy, and V. Koltun, "Vision transformers for dense prediction," in *Proceedings of the IEEE/CVF international conference on computer vision*, 2021, pp. 12179–12188.
- [26] S. S. Khan, P. K. Mishra, B. Ye, K. Newman, A. Iaboni, and A. Mihailidis, "Empirical thresholding on spatio-temporal autoencoders trained on surveillance videos in a dementia care unit," in *2023 20th Conference on robots and vision (CRV)*. IEEE, 2023, pp. 265–272.
- [27] N. Madan, N.-C. Ristea, R. T. Ionescu, K. Nasrollahi, F. S. Khan, T. B. Moeslund, and M. Shah, "Self-supervised masked convolutional

transformer block for anomaly detection,” *IEEE Transactions on Pattern Analysis and Machine Intelligence*, 2023.

- [28] J. Sun, X. Wang, N. Xiong, and J. Shao, “Learning sparse representation with variational auto-encoder for anomaly detection,” *IEEE Access*, vol. 6, pp. 33 353–33 361, 2018.
- [29] L. Pinheiro Cinelli, M. Araújo Marins, E. A. Barros da Silva, and S. Lima Netto, *Variational Autoencoder*. Cham: Springer International Publishing, 2021, pp. 111–149. [Online]. Available: https://doi.org/10.1007/978-3-030-70679-1_5
- [30] B. Gao, X. Kong, S. Li, Y. Chen, X. Zhang, Z. Liu, and W. Lv, “Enhancing anomaly detection accuracy and interpretability in low-quality and class imbalanced data: A comprehensive approach,” *Applied Energy*, vol. 353, p. 122157, 2024.
- [31] A. Manji, R. Basiri, F. Harton, K. Rommens, and K. Manji, “Effectiveness of a multidisciplinary limb preservation program in reducing regional hospitalization rates for patients with diabetes-related foot complications,” *The International Journal of Lower Extremity Wounds*, p. 15347346241238458, 2024.
- [32] R. Basiri, B. D. Haverstock, P. F. Petrusek, and K. Manji, “Reduction in diabetes-related major amputation rates after implementation of a multidisciplinary model: an evaluation in alberta, canada,” *Journal of the American Podiatric Medical Association*, vol. 111, no. 4, 2021.
- [33] X.-F. Han, H. Laga, and M. Bennamoun, “Image-based 3d object reconstruction: State-of-the-art and trends in the deep learning era,” *IEEE transactions on pattern analysis and machine intelligence*, vol. 43, no. 5, pp. 1578–1604, 2019.
- [34] K. Fu, J. Peng, Q. He, and H. Zhang, “Single image 3d object reconstruction based on deep learning: A review,” *Multimedia Tools and Applications*, vol. 80, no. 1, pp. 463–498, 2021.
- [35] AltumView, “Sentinare 2,” <https://altumview.ca/>, 2022, [Online; accessed 24-February-2022].
- [36] P. K. Mishra, A. Mihailidis, and S. S. Khan, “Skeletal video anomaly detection using deep learning: Survey, challenges, and future directions,” *IEEE Transactions on Emerging Topics in Computational Intelligence*, vol. 8, no. 2, pp. 1073–1085, 2024.



Bing Ye, received the MSc. at the Queen’s University, Canada. She has over 10 years research experience in aging and technology. Ye has been working as a Research Manager since 2016 in the Intelligent Assistive Technology and Systems Lab (IATSL) at the University of Toronto.



Kristine Newman obtained her Bachelor of Nursing Science (2003) and Master of Science in Nursing (2005) from Queen’s University. Dr. Newman completed her PhD in Nursing Science (2012) from the University of Toronto. She is a Professor at the Daphne Cockwell School of Nursing at Toronto Metropolitan University.



Pratik K. Mishra obtained his Masters in Computer Science and Engineering from the Indian Institute of Technology Indore, India, in 2020. He is currently pursuing his Ph.D. at the Institute of Biomedical Engineering, University of Toronto. His research is focused towards the application of deep learning for detecting behaviours of risk in patients living with dementia.



Alex Mihailidis, PhD, PEng, is the Barbara G. Stymiest Research Chair in Rehabilitation Technology at KITE Research Institute at University Health Network. He is the Scientific Director of AGE-WELL Network of Centres of Excellence, which focuses on development of new technologies and services for older adults. He is a Professor in the Department of Occupational Science and Occupational Therapy and in the Institute of Biomedical Engineering at the University of Toronto.



Irene Ballester is a PhD student and research assistant at the Computer Vision Lab at TU Wien, Austria. She is a Marie Curie ITN fellow for the visuAAL project, focusing on developing computer vision methods for measuring dementia behaviours. She obtained her Master in Industrial Technology Engineering (specialization in automation and robotics), from the University of Zaragoza, Spain in 2020.



Shehroz S. Khan obtained his B.Sc Engineering, Masters and Phd degrees in computer science in 1997, 2010 and 2016. He is currently working as a Scientist at KITE – Toronto Rehabilitation Institute, University Health Network, Canada. He is also cross appointed as an Assistant Professor at the Institute of Biomedical Engineering, University of Toronto.



Andrea Iaboni is a geriatric psychiatrist and clinician-scientist. She has a DPhil from Oxford University, UK (2002), and an MD from the University of Toronto, Canada (2006). She completed her residency in psychiatry (FRCPC, 2011) and a fellowship and sub-specialty in geriatric psychiatry (2013). She is an Associate Professor at the University of Toronto and a Senior Scientist at KITE-Toronto Rehab Institute, University Health Network, Toronto, Canada.